https://doi.org/10.22226/2410-3535-2023-1-28-32

Strain-rate dependent deformation behavior of additively manufactured stainless steel with different fractions of δ-ferrite

S. V. Astafurov, E. V. Melnikov, M. Yu. Panchenko†, K. A. Reunova, A. V. Luchin,
E. A. Zagibalova, E. G. Astafurova, E. A. Kolubaev

†panchenko.marina4@gmail.com

Institute of Strength Physics and Materials Science, SB of RAS, Tomsk, 634055, Russia

The effect of strain rate on the tensile deformation behavior of additively manufactured CrNi stainless steel with different fractions of δ-ferrite (14% in the as-built material and 6% after the post-built solid-solution treatment) was revealed with the focus on the deformation stage of macroscopic strain-induced γ→α' martensitic transformation. Tension tests were performed with the initial strain rates of 5×10^{-4}, 5×10^{-3}, and 5×10^{-2} s^{-1} at two different temperatures, at which slow (300 K) and fast (183 K) kinetics of martensitic transformation were realized. Post-built solid-solution treatment provided a partial dissolution of the δ-ferrite in the additively manufactured steel specimens and assisted higher strain hardening at the stage associated with γ→α' martensitic transformation. Independently on δ-ferrite fraction and test temperature, an increase in the strain rate weakly influences the stress and strain, at which the stage of macroscopic strain-induced transformation starts, but visibly decreases the strain hardening rate at this deformation stage. The latter testifies the slower kinetics of strain-induced martensitic transformation at higher strain rates.

Keywords: stainless steel, additive manufacture, δ-ferrite, strain-induced martensite, strain rate.

1. Introduction

Wire-feed electron beam additive manufacture (EBAM) is one of the cutting-edge industrial technologies for the fabrication of complex-shaped items due to the high deposition rate and good quality of the products. It is based on a layer-by-layer deposition of a metal wire with its simultaneous melting by electron beam as an energy source [1–4]. Chromium-nickel austenitic stainless steels are among the structural materials appropriate and widely adopted for additive manufacturing and, in particular, for the EBAM process [5–7]. In the additive manufacture, two main drawbacks are characteristic for austenitic stainless steels: the formation of an anisotropic grain structure (columnar coarse grains are elongated in the growth direction and crystallization texture forms) and high volume fraction of dendritic δ-ferrite in the microstructure (up to 20% of δ-phase in EBAM process, σ-phase also can form in other additive manufacture methods) [7–10]. A post-production heat treatment does not influence the grain size of the austenite but reduces the δ-phase fraction in EBAM-fabricated steels [8]. Unfortunately, a complete dissolution of the δ-ferrite could not be obtained by post-production heat treatments due to the partial depletion of the EBAM-fabricated billets by nickel during production [6,8,10].

Cold plastic deformation of the conventional CrNi steels with low stacking fault energies is accompanied with strain-induced γ→ε→α' or γ→α' martensitic transformations (MT) [11–14]. The strain-induced α'-martensite positively contributes to the strain hardening and plasticity of the steels in the low-temperature deformation regime. Moreover, the increase in flow stress at the deformation stage corresponding to the γ→α' or ε→α' transformation is directly proportional to the volume fraction of the α'-martensite [15]. The mechanisms and kinetics of the MTs are strongly dependent on both the structure of the steel (phase composition, grain size, stacking fault energy, texture, etc.) and deformation regime (strain rate, temperature, deformation mode, etc.) [11,12,15,16]. Therefore, thanks to the specific grain structure and dual phase composition, additively fabricated CrNi steels could possess the kinetics of the martensitic transformation different from the feedstock material (wire used for EBAM) or conventional steels (obtained by casting and solid-solution treatments).

In this paper, we study the effect of strain rate on the tensile deformation behavior of the additively manufactured CrNi stainless steel with different fractions of δ-ferrite at temperatures, where slow (300 K) or fast (183 K) kinetics of martensitic transformation is realized.

2. Materials and experimental methods

A wire-feed electron beam method was used to build a billet of stainless steel with the linear dimensions of $110\times33\times6$ mm^3 (Fig. 1). A 1.2 mm steel wire of type AISI 321 steel was used. The chemical composition of the wire and resultant composition of the EBAM-fabricated billet (central part) are given in Table 1.

The EBAM process was carried out in a vacuum chamber using the following parameters: beam accelerating voltage 30 kV, beam current 40 – 50 mA, scanning frequency 1 kHz,

wire-feed rate 3 mm/s, ellipse scan of 4.5×4.5 mm. The substrate was not cooled during the EBAM process.

For tensile tests, dumb-bell shaped flat specimens with the gauge sections of 12×2.6×1.4 mm (thickness) were cut from the EBAM-fabricated billet. The tensile axis coincided with the growth direction (perpendicular to the deposition direction and the substrate) (Fig. 1). A part of the specimens was subjected to a solid solution treatment (SST) for one hour at a temperature of 1100°C followed by water-quenching. Another part was studied in the initial (as-built) condition. Tensile specimens were mechanically ground using abrasive papers and electrochemically polished in a 50 g CrO_3 + 200 g H_3PO_4 solution. The tensile tests were performed at temperatures of 300 and 183 K and at initial strain rates of 5×10^{-4}, 5×10^{-3}, 5×10^{-2} s^{-1} (Instron 1185 testing system).

The microstructure of the specimens was analyzed using a Quanta 200 3D scanning electron microscope (SEM, BSD regime) equipped with an energy dispersion spectroscopy unit (EDS). A volume fraction of the initial δ-ferrite phase in specimens was measured at room temperature using a ferritometer MVP-2M (Kropus).

3. Results

Figure 2 shows the initial microstructure of the as-built and SS-treated specimens. All specimens possess mainly an austenitic structure. Dendritic δ-ferrite with the volume fraction of 14% and vermicular and lathy morphology is typical of EBAM-fabricated specimens (Fig. 2 a). After the SST, the former dendritic arms of δ-phase are still visible, but they are substantially dissolved. Separate rounded fragments of ferrite are seen in coarse austenitic grains (the fraction of δ-ferrite is 6%, Fig. 2 b). The features of the microstructure for as-built and SST-processed specimens are detailed in our previous paper [8].

Figure 3 represents "engineering stress vs. engineering strain" and "true stress vs. true strain" diagrams for the specimens tested in tension at two different temperatures.

Table 1. The chemical composition of the steel wire and EBAM-fabricated billet (central part).

Material	Concentration of the elements, mass. %						
	Cr	Ni	Mn	Ti	Si	C	Fe
Wire	17.7	9.7	1.1	0.8	0.6	0.08	balanced
EBAM-fabricated billet	17.5	9.5	0.6	0.8	0.7	0.08	balanced

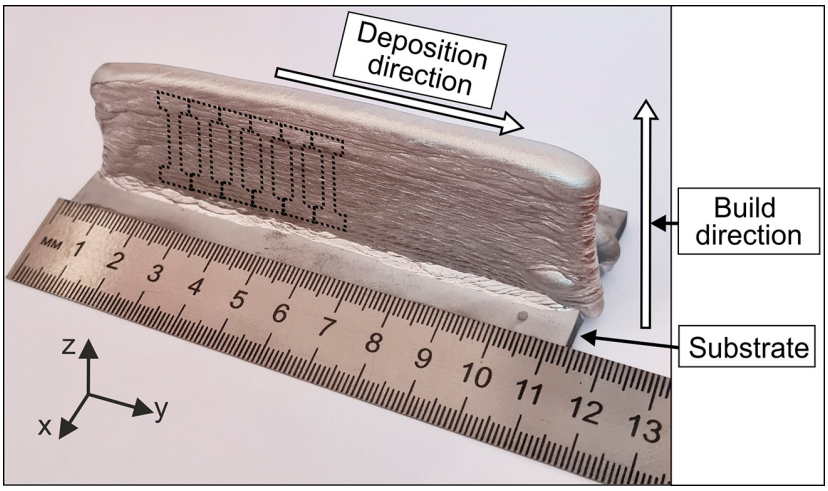

Fig. 1. (Color online) Image of EBAM-fabricated steel billet and schematic illustration showing the orientation of tensile specimens relative to the deposition and build direction.

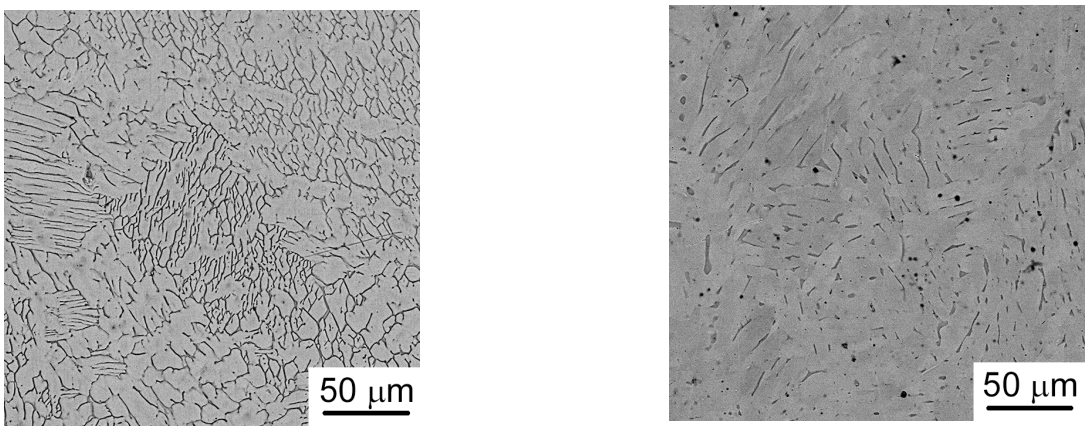

a b

Fig. 2. SEM images of the initial structures in the as-built (a) and SS-treated (b) specimens; light areas — austenite, dark areas — δ-ferrite.

For the low-temperature deformation regime, a transition from a parabolic (stage I) to a sigmoidal (stage II) strain hardening behavior at true strain about 0.1 is observed (T=183 K, Figs. 3 d, e). An increase in the strain hardening at deformation stage II (Figs. 4 a, b) is typically associated with a strain-induced martensitic transformation [11,12,17]. And, according to the data in Figs. 3 a, b, d, e, 4 a – c, the kinetics of the transformation is fast at this deformation temperature. At deformation stage II, the slopes $d\theta/d\sigma$, $d\theta/d\varepsilon$ and the absolute values of θ are higher in specimens with a lower fraction of δ-ferrite in comparison with those possessing a higher ferrite fraction (Fig. 4 c). Therefore, an increase in

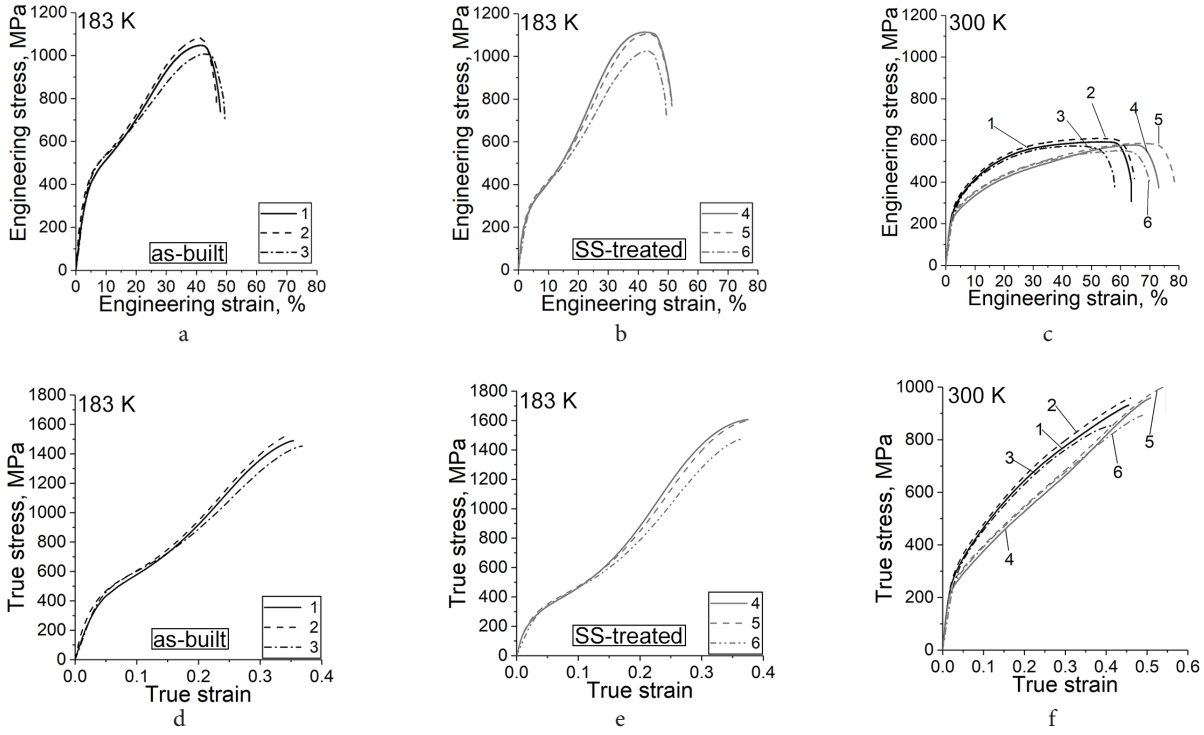

Fig. 3. Engineering stress vs. engineering strain (a – c) and true stress vs. true strain (d – f) diagrams for as-built (a, c, d, f) and SS-treated (b, c, e, f) steel specimens tensile tested at 183 K (a, b, d, e) and 300 K (c, f): (1) — 5×10^{-4} s^{-1}, as-built; (2) — 5×10^{-3} s^{-1}, as-built; (3) — 5×10^{-2} s^{-1}, as-built; (4) — 5×10^{-4} s^{-1}, SS-treated; (5) — 5×10^{-3} s^{-1}, SS-treated; (6) — 5×10^{-2} s^{-1}, SS-treated. The true stress-true strain diagrams in (d) to (f) were constructed using the corresponding engineering stress-strain diagrams in (a) to (c) except for the last deformation stage associated with the pre-fracture regime (macroscopic localization and neck formation).

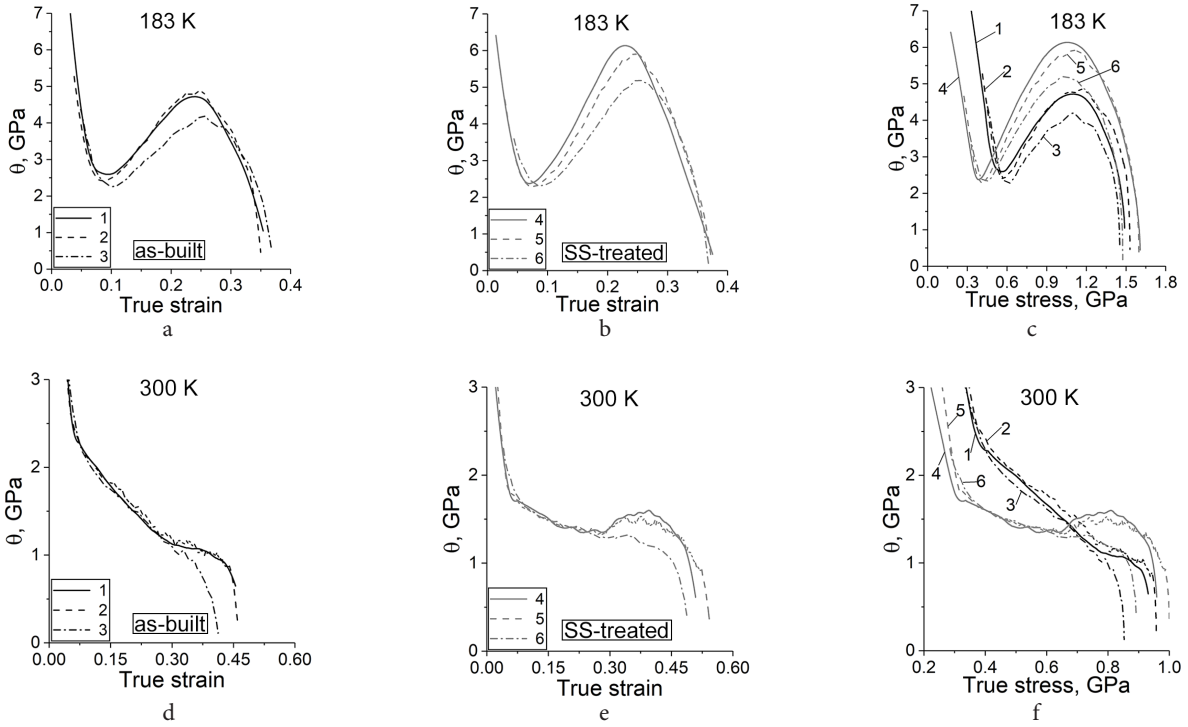

Fig. 4. Strain hardening coefficient $\theta = d\sigma/d\varepsilon$ vs. true strain (a, b, d, e) and vs. true stress (c, f) for as-built and SS-treated steel specimens tensile tested at 183 K (a, b, c) and 300 K (d, e, f): (1) — 5×10^{-4} s^{-1}, as-built; (2) — 5×10^{-3} s^{-1}, as-built; (3) — 5×10^{-2} s^{-1}, as-built; (4) — 5×10^{-4} s^{-1}, SS-treated; (5) — 5×10^{-3} s^{-1}, SS-treated; (6) — 5×10^{-2} s^{-1}, SS-treated.

the δ-ferrite fraction partially suppresses the strain-induced martensite nucleation and slows down the kinetics of martensitic transformation. For both types of the specimens, strain hardening at deformation stage II decreases when the strain rate increases, and the start of the stage II is slightly shifted to the higher stress and strains (Figs. 4 a – c).

In room temperature deformation, the stress-strain diagrams for as-built specimens are parabolic (Fig. 3 c, f). Stage II is short, but could be clearly revealed on dependences of the θ-value on the strain and stress (Figs. 4 d – f). These data show that the macroscopic strain-induced transformation at room temperature is shifted to higher strains and stresses, and its activity is substantially lower than that at the deformation temperature of 183 K. For the SST specimens tensile tested at 300 K, the stress-strain dependences look more linear and the increase of θ-value at stage II is more pronounced than that for the as-built specimens. The latter testifies more active strain-induced martensitic transformation in specimens with a lower fraction of δ-phase relative to the as-built specimens. The transformation is activated in them at similar strains but much lower stresses (about 650 MPa) in comparison with specimens with a higher δ-fraction. Nevertheless, the kinetics of the transformation at 300 K is weak for both types of the specimens. The θ-value at stage II is a strain-rate dependent characteristic, an increase in the strain rate decreases strain hardening in additively fabricated steel. Due to the slow transformation kinetics at 300 K, the stress and strain, at which strain-induced transformation starts, could hardly be determined with high accuracy using tensile data.

4. Discussion

Dendritic δ-ferrite is a typical phase of EBAM-fabricated CrNi stainless steel, and its volume fraction depends on both the additive manufacture regime and chemical composition of the feedstock material [7 – 9]. The boundaries of δ-phase effectively divide the coarse austenitic grains (200 – 300 μm in transverse sections and up to the several millimeters in length). Therefore, the dislocation free path is limited by the interphase boundaries rather than by grain boundaries of the austenite, and in both types of the specimens the grain-boundary strengthening (by interphase boundaries) is high. The higher volume fraction of the δ-ferrite provides a higher density of the interphase (γ/δ) boundaries and lower interdendritic distances (see Fig. 2). So, the higher yield strength and more parabolic strain hardening behavior at stage I in the as-built specimens is due to the higher volume fraction of the δ-phase in austenite. According to the previously reported data [11,12,15 –17], dislocation slip, twining and γ→ε phase transformation are dominating deformation mechanisms in this deformation stage.

At stage II of the strain hardening, the ε→α' or γ→α martensitic transformations are activated [11,12,15 –17]. In Figs. 3 a, b, d, e, the stress-strain diagrams show a deformation behavior typical of single-phase austenitic Cr-Ni steels with a strain-induced martensitic transformation [12,15,17]. The transition from a parabolic to sigmoidal strain hardening behavior at true strain about 0.1 is associated with a change in dominated deformation mechanisms from dislocation slip, twinning and γ→ε transformation at deformation stage I to the dislocation slip, twinning and ε→α' or γ→α' transformations at stage II [12 –17]. The more fraction of strain-induced α'-martensite is formed in the material, the higher the $d\theta/d\sigma$, $d\theta/d\varepsilon$ slopes [15,16]. Therefore, the $d\theta/d\sigma$ and $d\theta/d\varepsilon$ values directly represent the kinetics of the martensitic transformation from the austenite (or ε-martensite) to α'-martensite at stage II.

The comparison of the data in Figs. 4 a to 4 f for the strain rate of 5×10^{-4} s^{-1} shows that the SST-assisted decrease in the δ-ferrite fraction stimulates strain hardening and, therefore, strain-induced transformation. In the as-built specimens, it starts at higher stresses and possesses slower kinetics during plastic deformation. This is a non-obvious result, because a decrease in the grain size (interdendritic distances in our case) could either suppress the martensitic transformation and decrease the fraction of strain-induced martensite [18,19] or, contrarily, stimulate it [17]. A greater volume fraction of the α'-martensite was obtained in fine-grained type 304 stainless steel for the given strain level due to the high dislocation density and increased slip band interactions as compared to the coarse-grained material [17]. Contrarily, the authors of the paper [18] ascribe the higher fraction of the α'-martensite in coarser-grained AISI 304LN steel to the higher fraction of annealing twins, which are the preferred sites for a martensite nucleation, in their opinion. Our results support neither the first nor the second hypothesis. After tension at 183 K, the volume fraction of the α'-martensite in SST-processed specimens is 68 ± 2% against 57 ± 2% in as-built one (in part of the specimens, where uniform deformation was realized). The results of tensile tests in paper [18] lie in the line with our data — the structure with coarser austenitic regions is transformed faster and more completely —, but no annealing twins have been observed in additively fabricated specimens (Fig. 2 b). But, at the same time, the fraction of the transformed γ-phase is higher in SST-processed specimens due to the lower content of the initial δ-ferrite. Additionally, the morphology of the δ-phase has been changed during SST, which obviously influences the dislocation arrangement in austenite and the mechanisms of the α'-martensite nucleation and growth. Further investigations of the microstructure using transmission electron microscopy are needed to clarify these phenomena.

Strain-rate effect on the deformation behavior of the additively fabricated specimens is unusual as well. Independently on δ-ferrite fraction, an increase in the strain-rate is accompanied with a lowering of the slopes $d\theta/d\sigma$, $d\theta/d\varepsilon$. This result is controversial to that reported in [18] and supports the data of the paper [20]. Apparently, strain-induced martensitic transformation of additively manufactured material could not be described in terms of the direct effect of the grain size in austenitic steel and additively manufactured material should be considered as a dual-phase material (pseudo-composite) with hard inclusions (δ-ferrite) in a soft binder (austenite).

5. Conclusion

The strain rate-dependent deformation behavior of the additively manufactured CrNi stainless steel with different fractions of δ-ferrite (14% in the as-built material and 6%

after post-built solid-solution treatment) was investigated using tensile tests with the initial strain rates of 5×10^{-4}, 5×10^{-3}, and 5×10^{-2} s^{-1} at two different temperatures (183 and 300 K). A decrease in the δ-ferrite fraction assists higher strain hardening at the stage associated with macroscopic $\varepsilon\rightarrow\alpha'$, $\gamma\rightarrow\alpha'$ martensitic transformations. Independently on the δ-ferrite fraction and test temperature, an increase in the strain rate weakly influences the stress and strain, at which the stage of macroscopic transformation starts, but makes the kinetics of strain-induced martensitic transformation slower.

Acknowledgements. The study was carried out in accordance with the RF Government Assignment for the ISPMS SB RAS, Project No. FWRW-2022-0005. The investigations were performed using the equipment of the shared use center Nanotech (ISPMS SB RAS, Tomsk) and Tomsk State University (Tomsk Materials Science Center of Collective Use). The authors are grateful to cand. phys.-math. sciences V. E. Rubtsov and cand. phys.-math. sciences S. Yu. Nikonov for assistance in making the specimens.

References

1. D. Ding, Z. I. Pan, D. Cuiuri, H. Li. Int. J. Adv. Manuf. Technol. 81, 465 (2015). Crossref
2. I. Gibson, D. Rosen, B. Stucker, M. Khorasani. Additive Manufacturing Technologies, 3d edition. Springer (2021) 675 p. Crossref
3. E. A. Kolubaev, V. E. Rubtsov, A. V. Chumaevskii, E. G. Astafurova. Physical Mesomechanics. 25 (4), 5 (2022). (in Russian) Crossref
4. D. Svetlizky, M. Das, B. Zheng, A. L. Vyatskikh, S. Bose, A. Bandyopadhyay, J. M. Schoenung, E. J. Lavernia, N. Eliaz. Mater. Today. 49, 271 (2021). Crossref
5. D. Herzog, V. Seyda, E. Wycisk, C. Emmelmann. Acta Mater. 117, 371 (2016). Crossref
6. S. Astafurov, E. Astafurova. Metals. 11 (7), 1052 (2021). Crossref
7. P. Bajaj, A. Hariharan, A. Kini, P. Kürnsteiner, D. Raabe, E. A. Jägle. Mater. Sci. Eng. A. 772, 138633 (2020). Crossref
8. E. G. Astafurova, M. Yu. Panchenko, V. A. Moskvina, G. G. Maier, S. V. Astafurov, E. V. Melnikov, A. S. Fortuna, K. A. Reunova, V. E. Rubtsov, E. A. Kolubaev. J. Mater. Sci. 55, 9211 (2020). Crossref
9. E. G. Astafurova, V. A. Moskvina, M. Yu. Panchenko, S. V. Astafurov, E. V. Melnikov, G. G. Maier, K. A. Reunova, V. E. Rubtsov, E. A. Kolubaev. Russian Phys. J. 63, 6 (2020). Crossref
10. E. V. Melnikov, E. G. Astafurova, S. V. Astafurov, G. G. Maier, V. A. Moskvina, M. Y. Panchenko, S. V. Fortuna, V. E. Rubtsov, E. A. Kolubaev. Letters on Materials. 9 (4), 460 (2019). Crossref
11. Martensite (ed. by G. B. Olson, W. S. Owen). ASM International (1992) 331 p.
12. K. Spencer, M. Veron, K. Yu-Zhang, J. D. Embury. Mat. Sci. Techn. 25, 7 (2009). Crossref
13. D. Kaoumi, J. Liu. Mater. Sci. Eng. A. 715, 73 (2018) Crossref
14. V. E. Ol'shanetskii, G. V. Snezhnoi, V. L. Snezhnoi. Met. Sci. Heat Treat. 60 (3-4), 165 (2018). Crossref
15. V. Seetharaman, R. Krishnan. J. Mater. Sci. 16, 523 (1981). Crossref
16. I. V. Kireeva, Yu. I. Chumlyakov. Mater. Sci. Eng. A. 481–482, 737 (2008). Crossref
17. K. De, J. G. Speer, D. K. Matlock. Metall. Mater. Trans. A. 37A, 1875 (2006). Crossref
18. S. Ganesh Sundara Raman, K. A. Padmanabhan. J. Mater. Sci. Lett. 13, 389 (1994). Crossref
19. Y. Hong, C. Zhou, Y. Zheng, L. Zhang, J. Zheng, X. Chen, B. An. Mater. Sci. Eng. A. 740, 420 (2019). Crossref
20. N. I. Vázquez-Fernández, T. Nyyssönen, M. Isakov, M. Hokka, V. T. Kuokkala. Acta Mater. 176, 134 (2019). Crossref